Supporting Information

Water-soluble carbon dots with blue, yellow and red emissions: mechanism investigation and array based fast sensing application

Yuanyuan Liu[1], Jian Zhang[2], Xuan Zhao[1], Wentao Li[1], Jun Wang[1], Yuhuan Gao[1],Yanyun Cui[3], Shenghao Xu[1,*], Xiliang Luo[1,*]

[1] Key Laboratory of Optic-electric Sensing and Analytical Chemistry for Life Science，MOE; College of Chemistry and Molecular Engineering, Qingdao University of Science and Technology, Qingdao 266042, P. R. China.

[2] College of Chemical Engineering, Qingdao University of Science and Technology, Qingdao 266042, PR China

[3] School of Science, Beijing Technology and Business University, Beijing 100048, P. R. China

[*]**Corresponding author:**

Shenghao Xu (xushenghao@qust.edu.cn); Xiliang Luo (xiliangluo@qust.edu.cn)

Key Laboratory of Optic-electric Sensing and Analytical Chemistry for Life Science, MOE; College of Chemistry and Molecular Engineering. Qingdao University of Science and Technology, Qingdao 266042, P. R. China.

List of Contents

Materials and Methods

Materials

m-Phenylenediamine (mPD), o-Phenylenediamine (oPD), p-Phenylenediamine (pPD), $FeCl_3$, homocysteine (Hcy), L-cysteine (Cys), reduced glutathione (GSH), methionine (Met), cystine, oxidized glutathione (GSSG), N-acetyl-L-cysteine (NAC), Na_2S, $Na_2S_2O_8$, $Na_2S_2O_3$, $AgNO_3$ and $CrCl_3 \cdot 6H_2O$ were purchased from Sigma-Aldrich. Ultrapure water (18 MΩ cm) from a Millipore Simplicity water purification system (Millipore) was utilized for preparing all solutions. Serum samples of rectal cancer patients, breast cancer patients, prostate cancer patients, and healthy people were obtained from the Eighth Peoples' Hospital of Qingdao with informed consent from the human subjects. In addition, sample collection was approved by Institutional Review Board of Eighth Peoples' Hospital of Qingdao. Standard strains of Escherichia coli (BNCC 336686), Aspergillus niger (BNCC 186380), Staphylococcus albus Rosenbach, Thiobacimonas profunda and Bosea thiooxidans were purchased from Beina Chuanglian Biology Research Institute (Shang Cheng).

Instruments

All fluorescence spectra were collected using a FLS1000 fluorescence spectrometer (Edinburgh, U.K.). A VILBER bioimaging system was used to obtain the fluorescence images (Quantum, France). X-ray photoelectron spectroscopy (XPS) was performed on an ESCALAB 250 X-ray photoelectron spectrometer (ThermoFisher). FT-IR was performed on a FT/IR-410 Fourier transform-infrared spectrophotometer (JASCO, Japan). Transmission electron microscopy (TEM) was performed by a JEOL JEM-2100 microscope (Japan). Raman spectroscopy was measured on a Renishaw Invia Raman microscope system with 633 nm laser excitation.

Synthesis of three kinds of multiple-color-emissive CDs

For blue emitting CDs (m-CDs), 10 mL of 16 mM mPD and 50 μL of 100 mM $FeCl_3$ were added to 90 mL of deionized water. The mixture was placed at 90 °C without stirring for 10 h. Then, the crude products were centrifugated at 12000 rpm for 15 min to remove large aggregates and the m-CDs were obtained. For yellow emitting CDs (o-CDs), 10 mL of 16 mM oPD and 50 μL of 100 mM $FeCl_3$ were added to 90 mL of deionized water. The mixture was placed at 90 °C without stirring for 10 h. Then, the crude products were centrifugated at 12000 rpm for 15 min to remove large aggregates and the o-CDs were obtained. For red emitting CDs (p-CDs), 10 mL of 16 mM pPD and 50 μL of 100 mM $FeCl_3$ were added to 90 mL of deionized water. The mixture was placed at 90 °C without stirring for 10 h. Then, the crude products were centrifugated at 12000 rpm for 15 min to remove large aggregates and the p-CDs were obtained. All these three CDs were stored at 4 °C before use.

DFT calculation

DFT theoretical calculation was performed by the tool of Vienna ab initio simulation package (VASP). The generalized gradient approximation (GGA), the perdew-burke-ernzerhof (PBE) exchange–correlation functional, and the ultrasoft pseudopotential were employed in the calculations. The cutoff energy was set to be 380 eV, and structure relaxation was performed until the convergence criteria of energy and force reached $1*10^{-5}$ eV and 0.03 eV $Å^{-1}$, respectively. Monkhorst-Pack meshes of 3*3*1 k-points were used to sample the two-dimensional brillouin zone for geometry optimization and electronic structure calculations, respectively.

SP-DFT calculation

SP-DFT calculation was carried out under the scheme of generalized gradient approximation, with the use of PBE functional and double numerical polarized basis, as embedded in DMol3 package. Geometry and energy calculations were converged with total energy change less than 10^{-4}

eV and the force on each atom being less than 0.05 eV/Å for convergence criterion. Quantum dots were modelled by cluster models, derived from graphene monolayers. Specifically, a series of clusters with different N-dopants were generated, which contain three locations for these N-dopants, namely meta-, ortho- and para-positions, being labelled as m-, o- and p-.

Sulfur species discrimination

Firstly, m-CDs (1/2), o-CDs (1/15) and p-CDs (1/10) were obtained through diluting the corresponding stocks using deionized water, respectively. Then, 0.6 μL Ag^{+} (100 mM) was added to 200 μL m-CDs (1/2), 0.45 μL Cr^{3+} (100 mM) was added to 200 μL o-CDs (1/15), 0.45 μL Cr^{3+} (100 mM) was added to 200 μL p-CDs (1/10), respectively. Afterthat, 200 μL of the above quenched solutions were added to each hole of the 96-well plate, respectively. Subsequently, 5.0 μL of 1.0 mM different sulfur species were added to each hole, respectively, and reacted at room temperature for 2 min. At last, bioimaging system were used to obtain the fluorescent response data and principal component analysis (PCA) was utilized to transform these fluorescence response data to the 2-dimensional plot for multidimensional analysis.

Cancer serum and bacteria discrimination

0.6 μL Ag^{+} (100 mM) was added to 200 μL m-CDs (1/2), 0.45 μL Cr^{3+} (100 mM) was added to 200 μL o-CDs (1/15), 0.45 μL Cr^{3+} (100 mM) was added to 200 μL p-CDs (1/10), respectively. Afterthat, 200 μL of the above quenched solutions were added to each hole of the 96-well plate, respectively. For serum discrimination, 5.0 μL of serums from rectal cancer, breast cancer, prostate cancer patients and healthy people were then added to each hole, respectively, and reacted at room temperature for 2 min. For bacteria discrimination, 5.0 μL of different bacteria were added to each hole, respectively, and reacted at room temperature for 2 min. At last, bioimaging system were used

to obtain the fluorescent response data and PCA was utilized to transform these fluorescence response data to the 2-dimensional plot for multidimensional analysis.

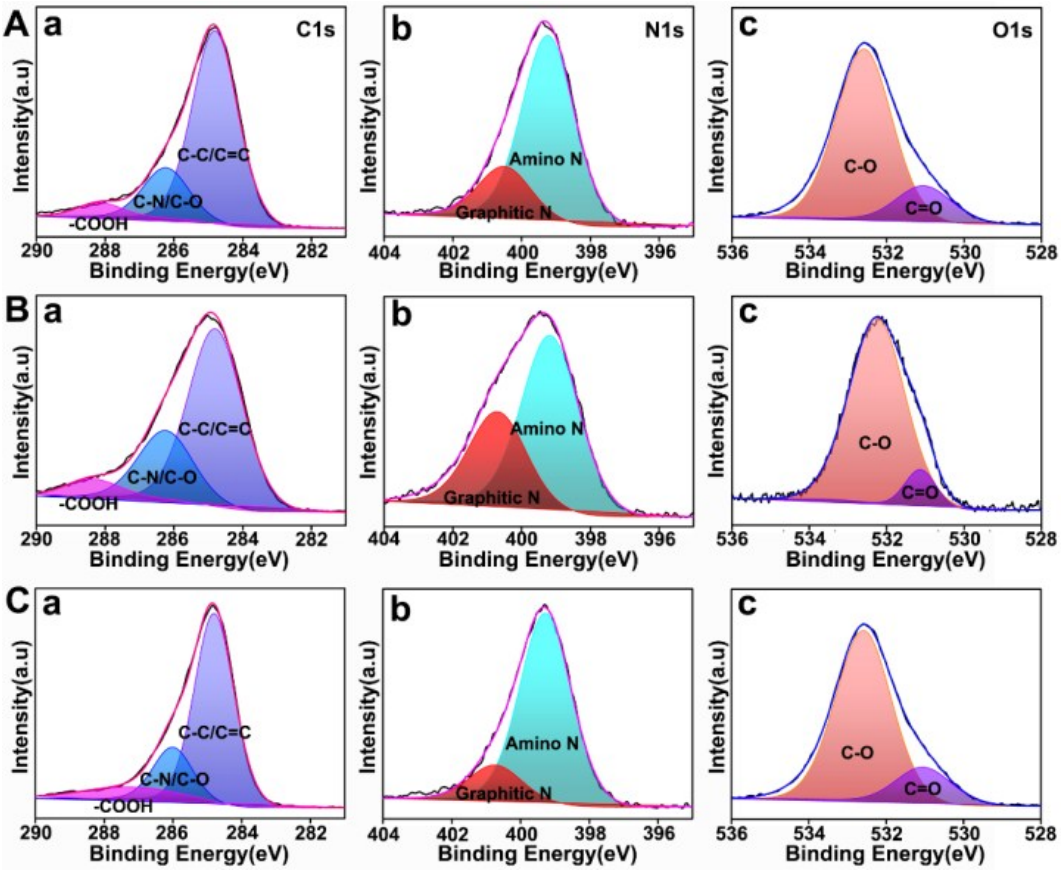

Fig. S1 High-resolution C1s, N1s and O1s XPS spectra for (A) m-CDs, (B) o-CDs and (C) p-CDs, respectively.

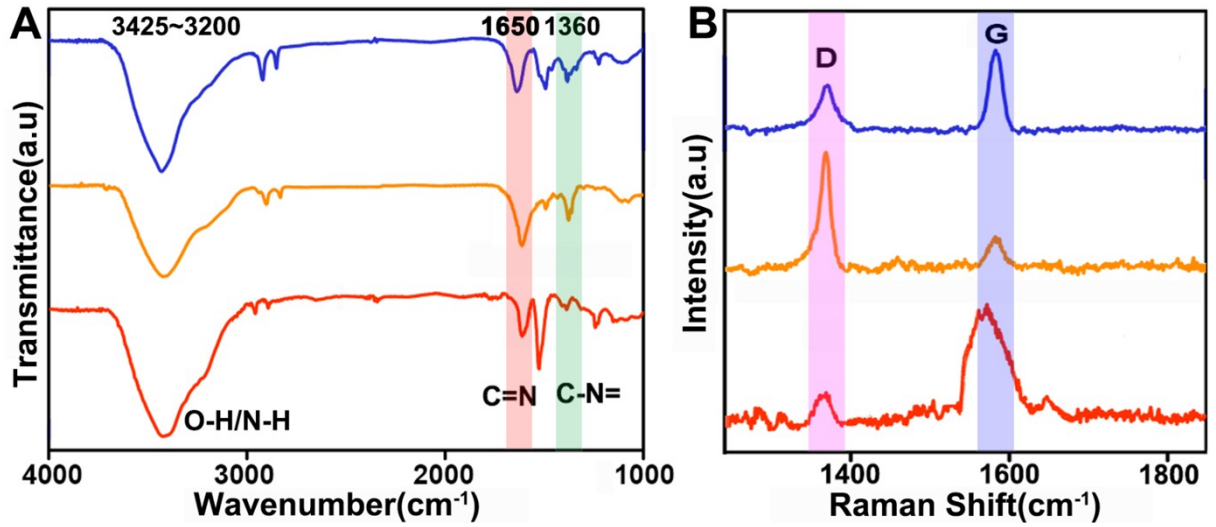

Fig. S2 (A) FT-IR and (B) raman spectra of m-CDs, o-CDs and p-CDs, respectively.

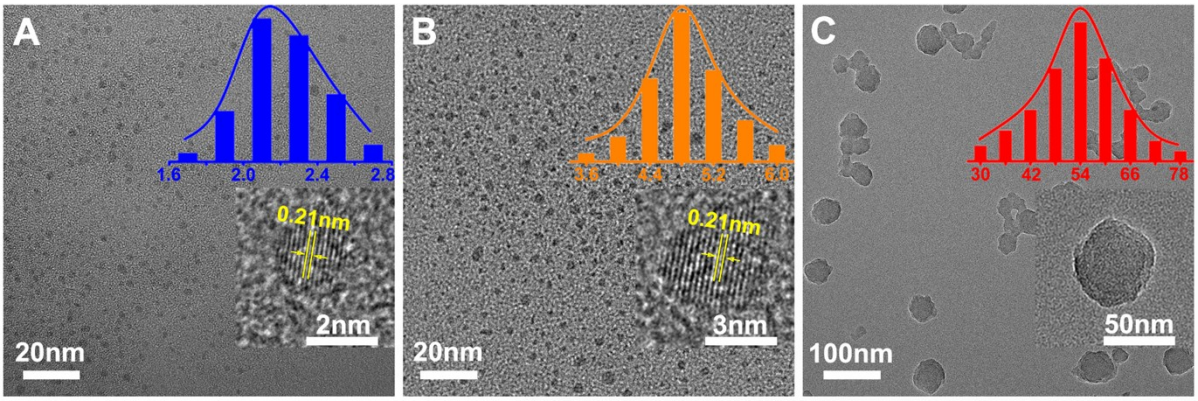

Fig. S3 TEM images of (A) m-CDs, (B) o-CDs and (C) p-CDs, respectively. Insets (bottom) are the corresponding high resolution transmission electron microscope (HRTEM), respectively.

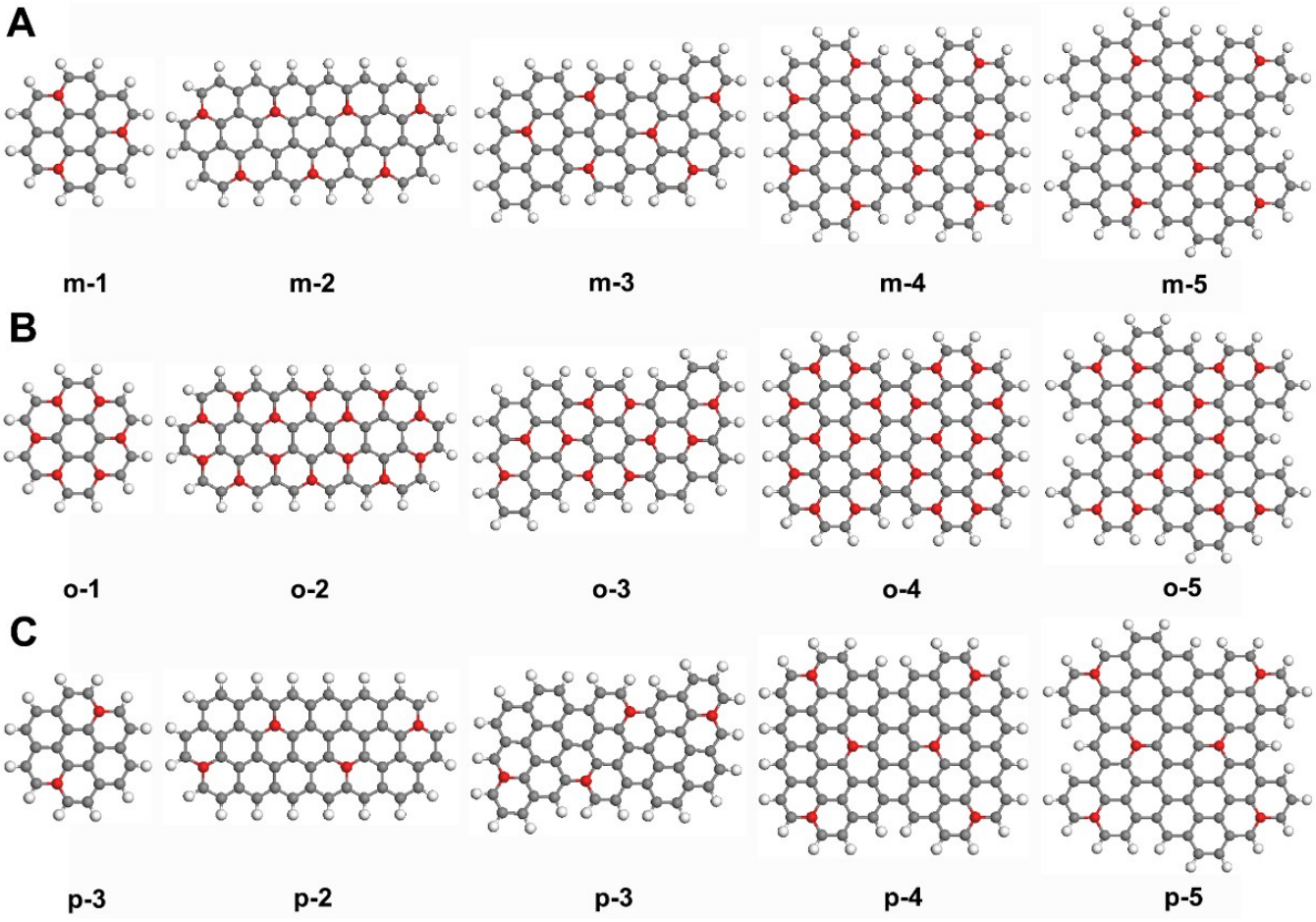

Fig. S4 Five models of the self-polymerization of three monomers (mPD, oPD and pPD) to form (A) m-CDs, (B) o-CDs and (C) p-CDs with different sizes established using SP-DFT calculation.

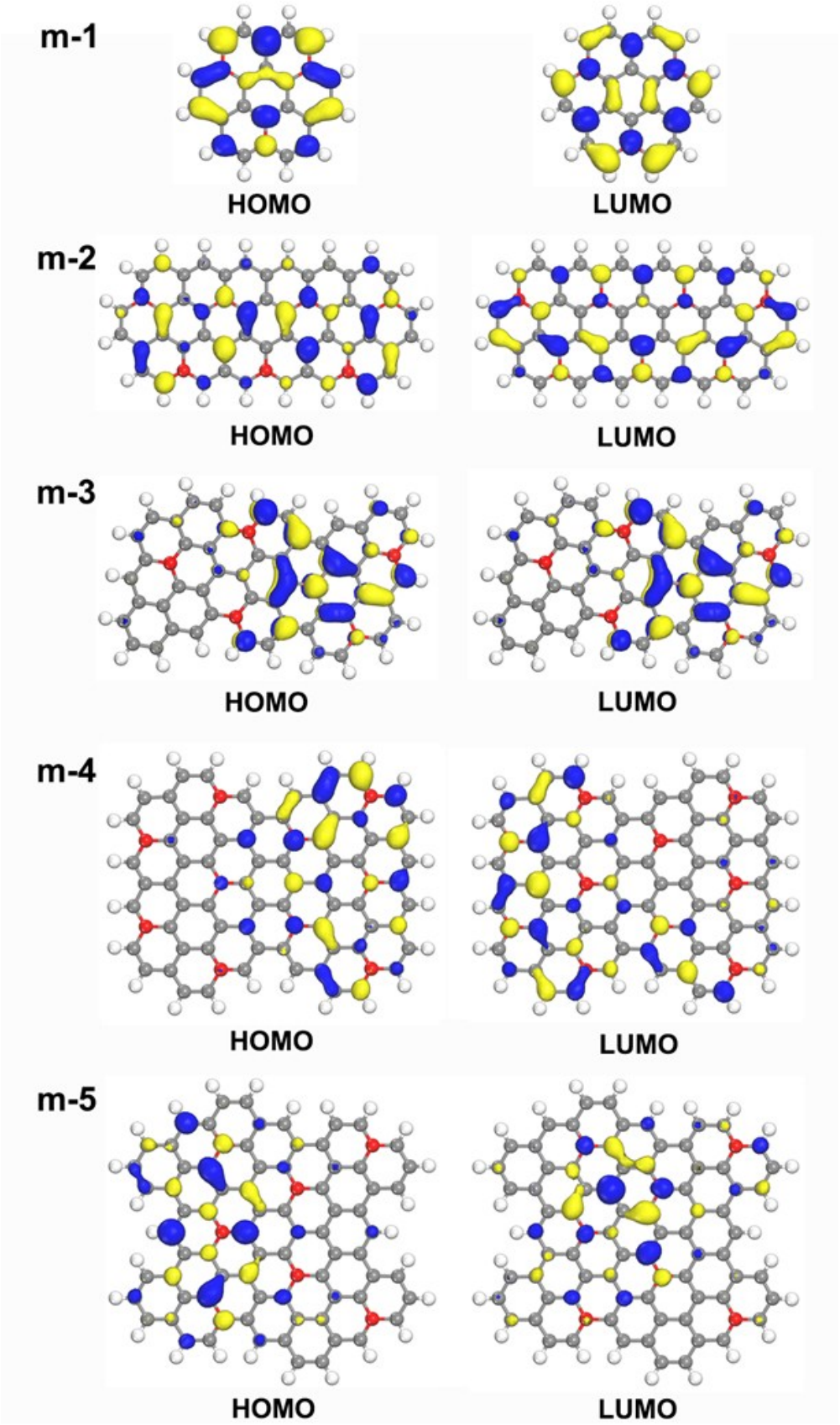

Fig. S5 HOMO and LUMO calculated molecular orbitals of the self-polymerization of mPD to form m-CDs with different sizes.

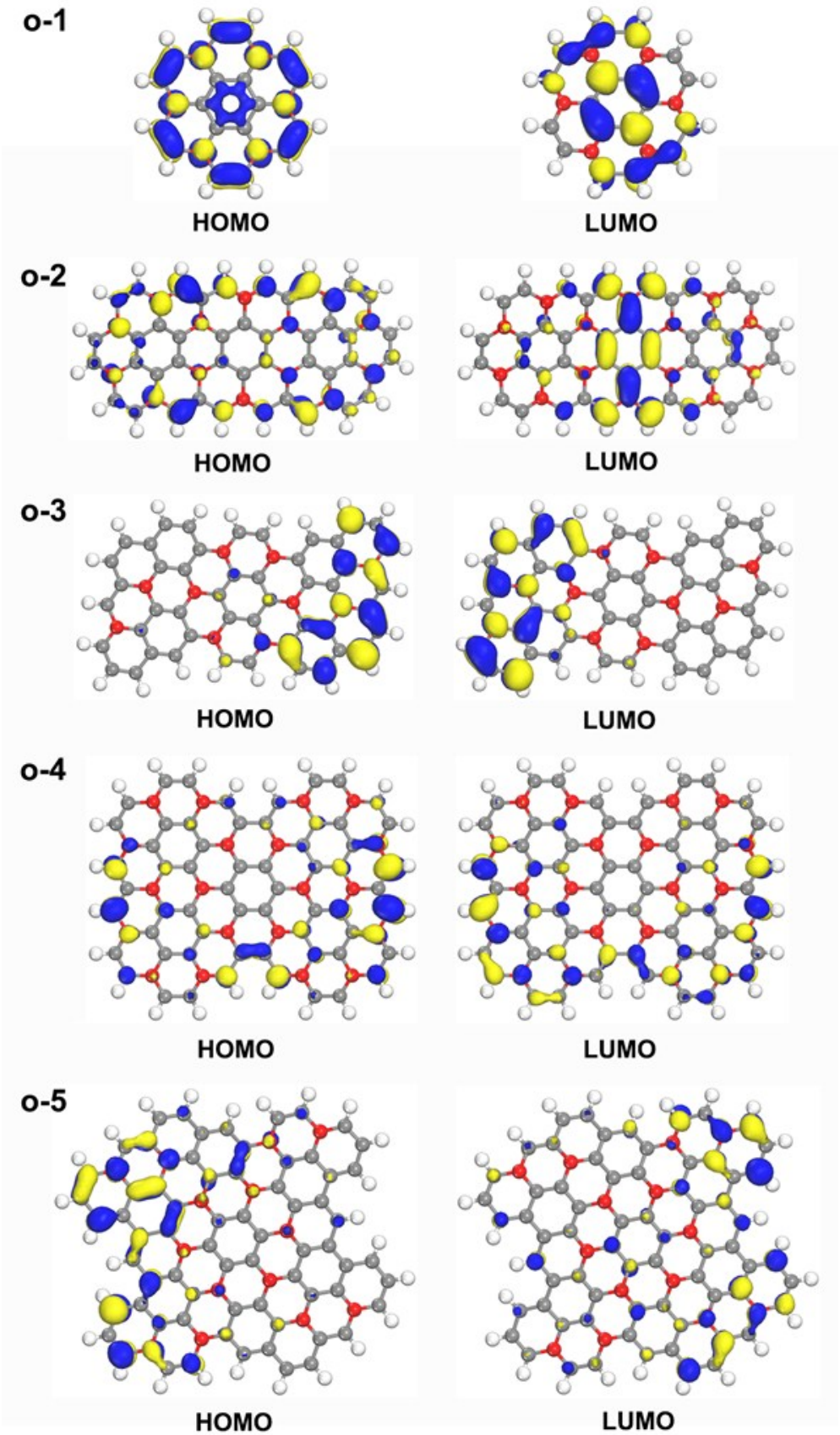

Fig. S6 HOMO and LUMO calculated molecular orbitals of the self-polymerization of oPD to form o-CDs with different sizes.

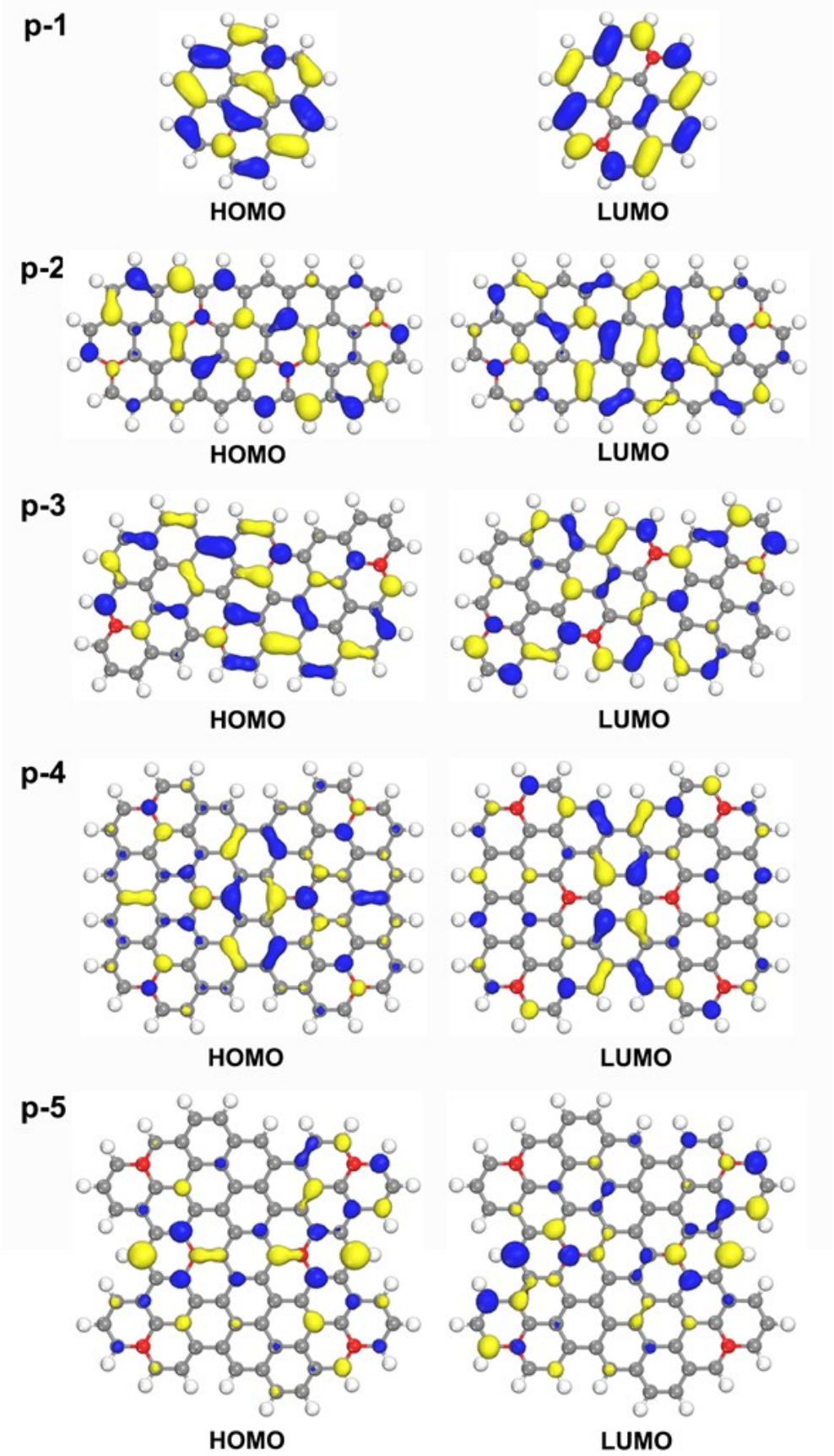

Fig. S7 HOMO and LUMO calculated molecular orbitals of the self-polymerization of pPD to form p-CDs with different sizes.

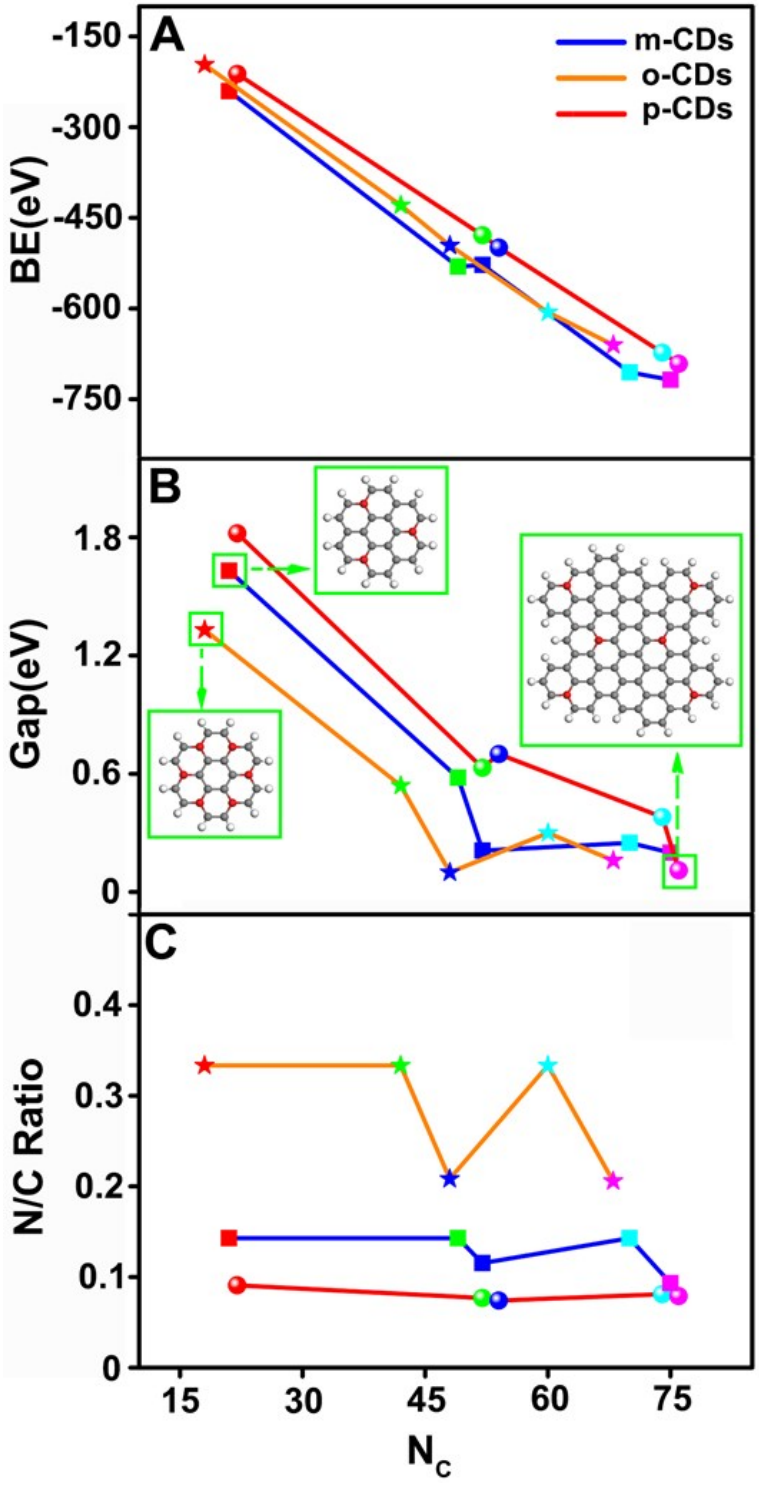

Fig. S8 Calculated properties of N-doped CDs. (A) Binding energies for the self-polymerization of three monomers (mPD, oPD and pPD) to form m-CDs, o-CDs and p-CDs with different sizes, respectively. (B) HOMO-LUMO gaps and (C) the dopping amount of graphite N for m-CDs, o-CDs and p-CDs with different sizes, respectively. Here, the number of carbon (NC) indicates the different size of these CDs

For the sensor array, the function of Ag^{+} and Cr^{3+} is as a bridge to induce the aggregation of CDs, leading to the fluorescence quenching. According to reported literatures, functional groups (e.g.,

carboxyl or amino groups) on the surface of CDs could chelate Ag^+ and Cr^{3+} with high coordination.[S1,S2] Therefore, as shown in **Fig. S9A**, Ag^+ can act as a bridge to induce the aggregation of m-CDs, resulting in the aggregation-induced fluorescence quenching. Similarly, the fluorescence of o-CDs and p-CDs can also be quenched because of Cr^{3+} induced aggregation (**Fig. S9B** and **Fig. S9C**). However, because of the competitive binding, these aggregated CDs redispersed after the addition of sulfur-containing species (using GSH as an example, **Fig. S9D** to **F**) and resulted in the fluorescence recovery. Overall, adding the same sulfur-containing species to these three quenched CDs would generate different fluorescence recoveries. Adding different sulfur-containing species to the same quenched CDs would also generate different fluorescence recoveries. In addition, it's worth noting that sulfur-containing species had no effect on the fluorescence of these three CDs (**Fig. S10**). Therefore, pattern recognition of different sulfur-containing species will be achieved according to these different cross fluorescence responses (**Fig. S11**). In addition, in addition to these two ions, some other ions such as Co^{2+}, Zn^{2+}, Mn^{2+}, Cd^{2+}, Ni^{2+} and Hg^{2+} were also investigated. As shown in **Fig S12 A B** and **C**, Ag^+, Cr^{3+} and Hg^{2+} both can cause fluorescence quenching of CDs. However, after adding different kinds of sulfur-containing species (using Na_2S, Met and GSH as an example) to the Hg^{2+} induced quenching system, there was no significant fluorescence recovery. Contrastively, obvious fluorescence recovery can be observed after adding different kinds of sulfur-containing species (using Na_2S, Met and GSH as an example) to the Ag^+ and Cr^{3+} induced quenching system, respectively. Therefore, Ag^+ and Cr^{3+} were selected to construct the sensor array.

S1 Y. P. Wu, X. Liu, Q. H. Wu, J. Yi, G. L. Zhang, *Anal. Chem.,* 2017, **89**, 7084-7089.

S2 S. Chen, C. H. Xu, Y. L. Yu, J. H. Wang, Sens. *Actuators B Chem.*, 2018, **266**, 553-560.

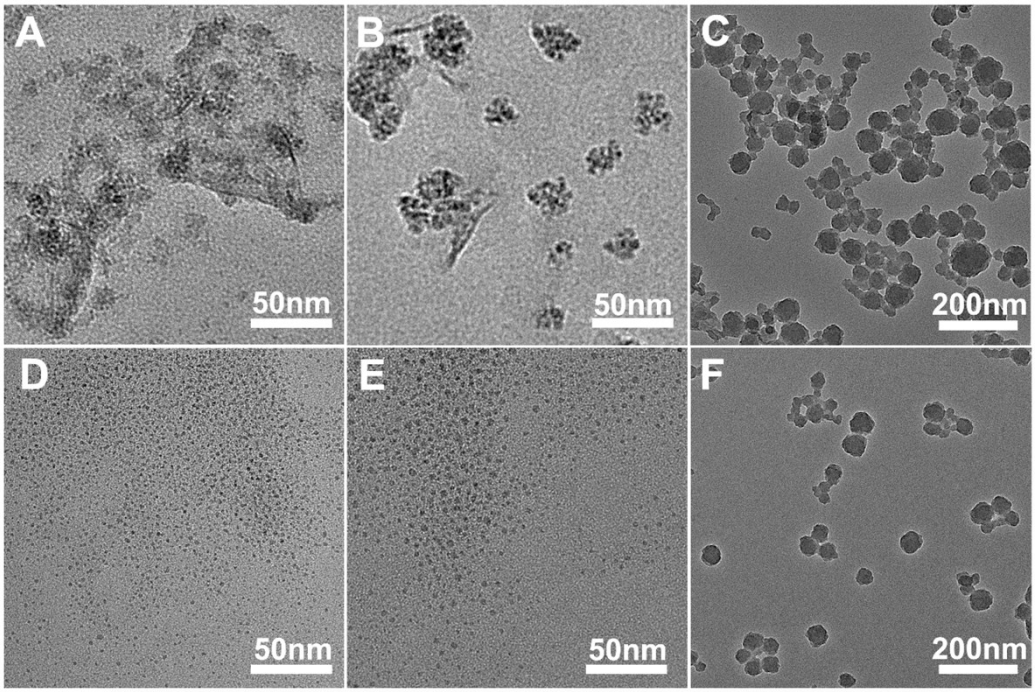

Fig. S9 TEM images of (A) m-CDs-Ag^{+} complex, (B) o-CDs-Cr^{3+} complex and (C) p-CDs-Cr^{3+} complex, respectively. TEM images of (D) m-CDs-Ag^{+} complex, (E) o-CDs-Cr^{3+} complex and (F) p-CDs-Cr^{3+} complex after adding GSH, respectively.

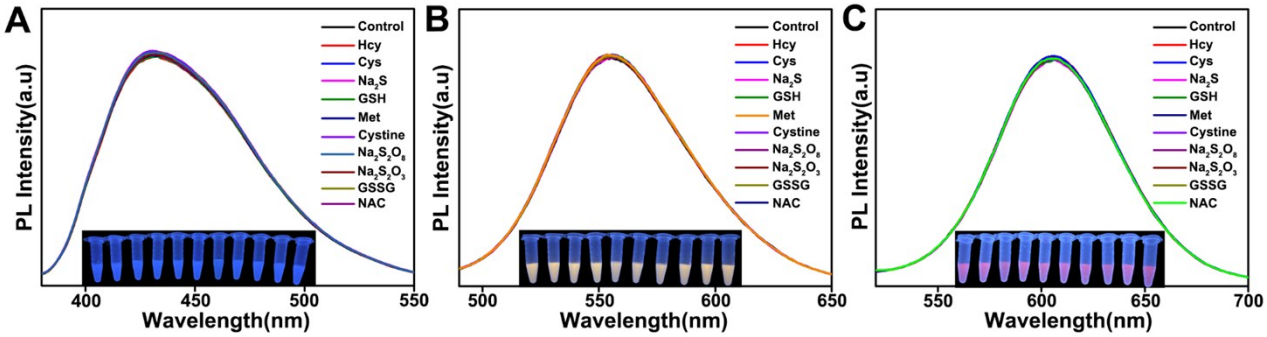

Fig. S10 Fluorescence spectra of (A) m-CDs, (B) o-CDs and (C) p-CDs in the presence of various sulfur-containing species, respectively.

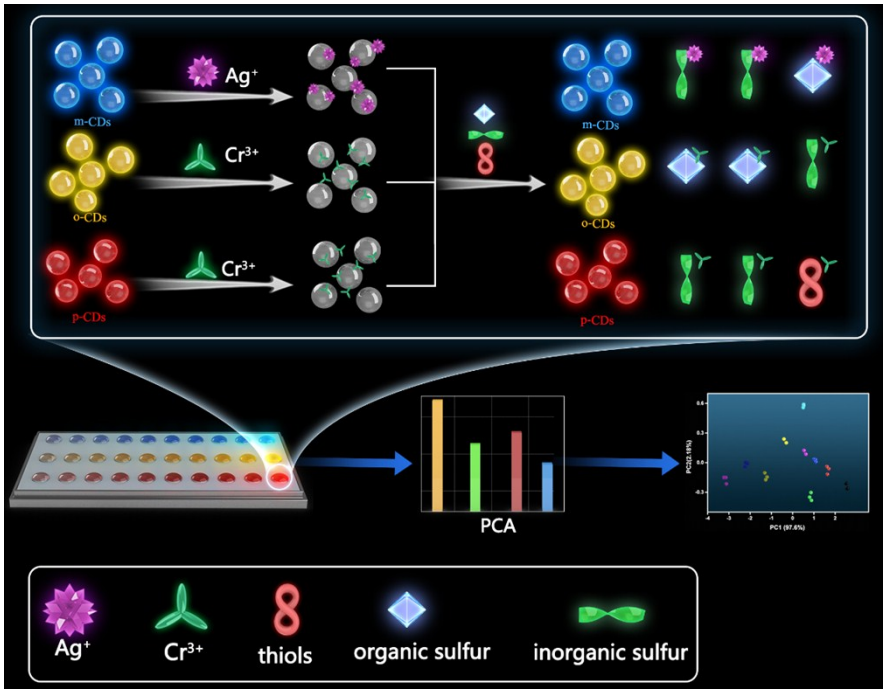

Fig. S11 Schematic illustration of the array based multidimensional platform for sulfur species discrimination using CDs- metal ion complex.

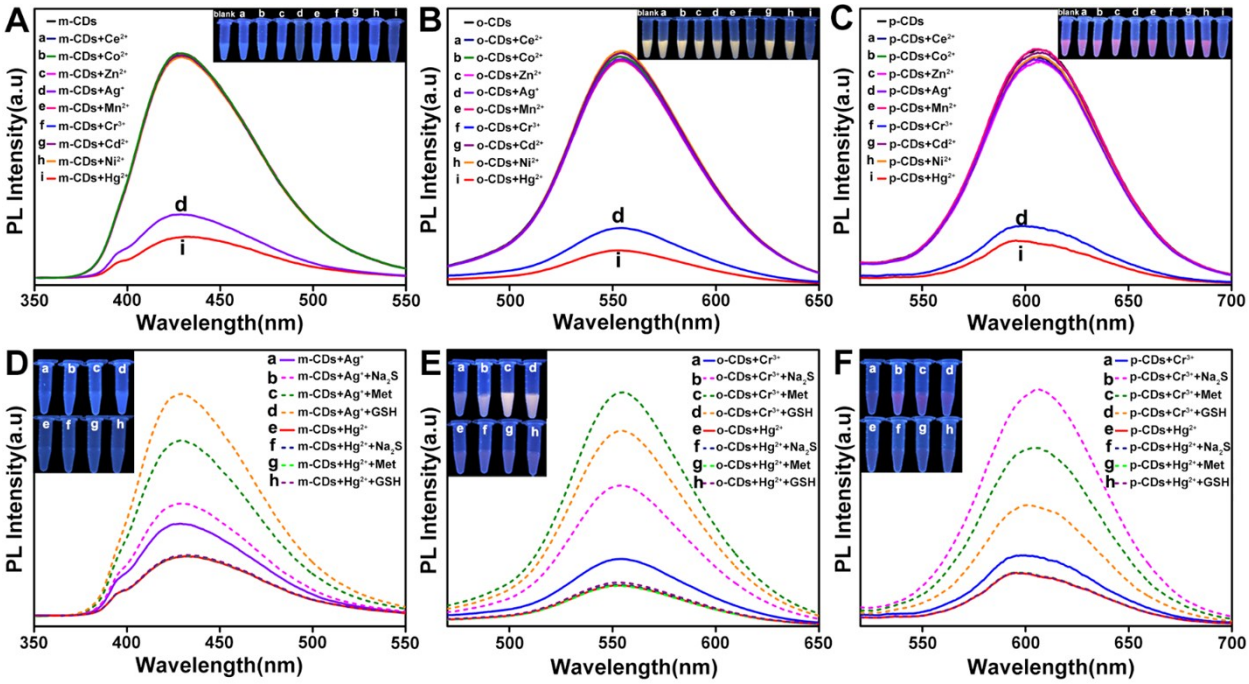

Fig. S12 Fluorescence spectra of (A) m-CDs, (B) o-CDs and (C) p-CDs in the presence of Co^{2+}, Zn^{2+}, Ag^{+}, Mn^{2+}, Cr^{3+}, Cd^{2+}, Ni^{2+} and Hg^{2+}, respectively. Fluorescence spectra of (D) m-CDs-Ag^{+}, m-CDs-Hg^{2+}, (E) o-CDs-Cr^{3+}, o-CDs-Hg^{2+} and (F) p-CDs-Cr^{3+}, p-CDs-Hg^{2+} in the presence of Na_2S, Met and GSH, respectively. The insets are the corresponding fluorescent photoes under the ultraviolet lamp.

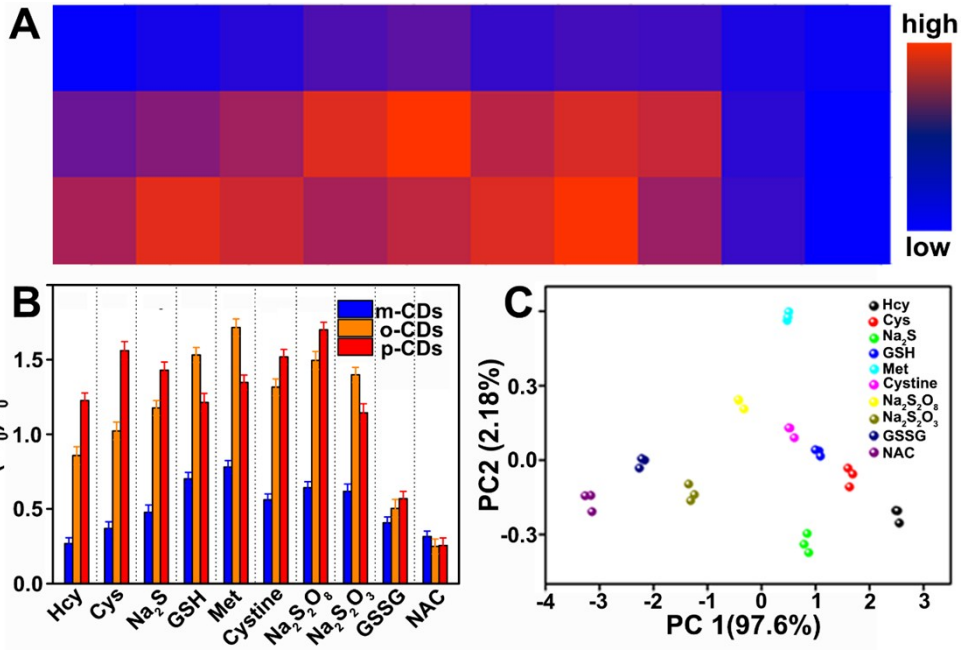

Fig. S13 (A) Heat map derived from the corresponding fingerprint-like patterns. (B) Fluorescence response of the CDs-metal ion based multidimensional platform against various sulfur-containing species (25 μM), in which I and I_0 represent the fluorescence intensities of CDs-metal ion complex in the presence and absence of sulfur-containing species, respectively. (C) PCA plot for the discrimination of the sulfur-containing species.

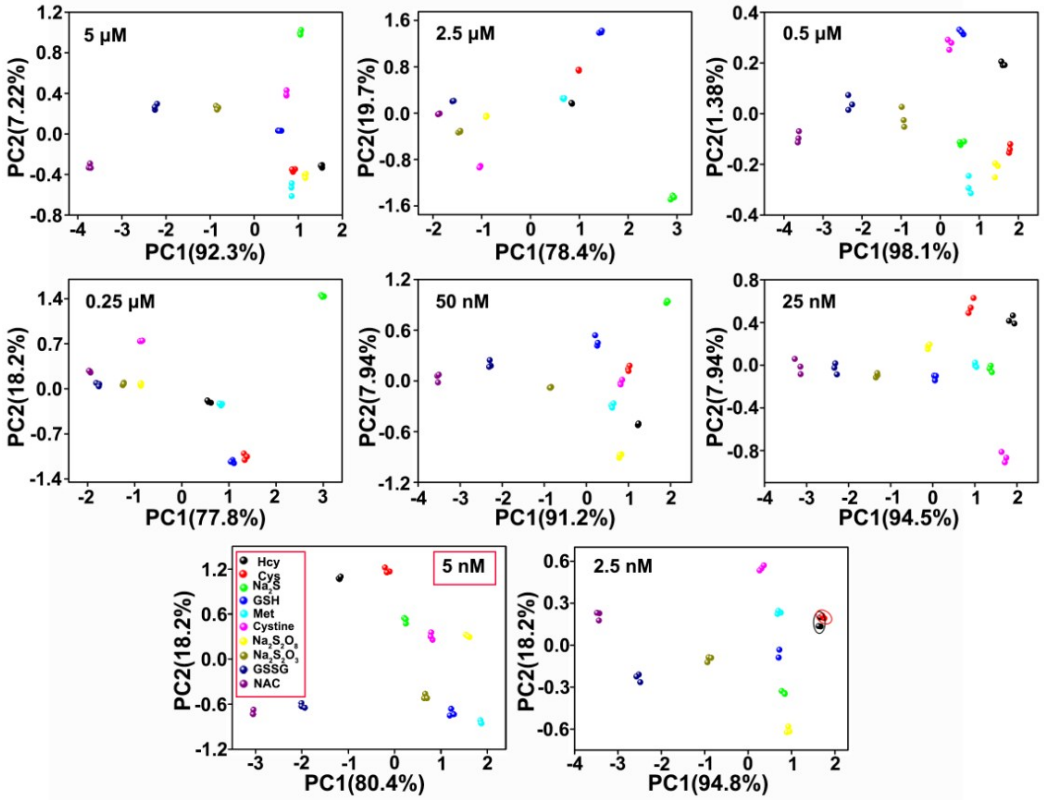

Fig. S14 PCA plot for the discrimination of sulfur-containing species at different concentrations.

Table S1. Relative fluorescence increase$(I-I_0)/I_0$

m-CDs	o-CDs	p-CDs	Identi.	Verifi.
0.315896832	0.22824349	0.288246881	NAC	NAC
0.485789402	1.172453175	1.438097323	Na_2S	Na_2S
0.617152441	1.398526725	1.14445174	$Na_2S_2O_3$	$Na_2S_2O_3$
0.612710213	1.404979443	1.168454075	$Na_2S_2O_3$	$Na_2S_2O_3$
0.654956711	1.489093193	1.71540089	$Na_2S_2O_8$	$Na_2S_2O_8$
0.314718281	0.2484582	0.255635807	NAC	NAC
0.582883822	1.289001827	1.511198658	Cystine	Cystine
0.622183945	1.420169027	1.158094404	$Na_2S_2O_3$	$Na_2S_2O_3$
0.477992838	1.17639333	1.429415627	Na_2S	Na2S
0.642400616	1.495431704	1.700517984	$Na_2S_2O_8$	$Na_2S_2O_8$
0.379810525	1.038145272	1.548114102	Cys	Cys
0.663161235	1.480470534	1.729262421	$Na_2S_2O_8$	$Na_2S_2O_8$
0.407778433	0.504396985	0.568979354	GSSG	GSSG
0.389873532	1.031692554	1.578171737	Cys	Cys
0.428267078	0.497601645	0.579849712	GSSG	GSSG
0.707402203	1.560244404	1.238710148	GSH	GSH
0.560627351	1.315326633	1.518348289	Cystine	Cystine
0.691627759	1.552364093	1.243962939	GSH	GSH
0.569149177	1.298595249	1.504997447	Cystine	Cystine
0.323058792	0.22144815	0.269497337	NAC	NAC
0.776483387	1.728529009	1.339169767	Met	Met
0.258691809	0.879568296	1.211716641	Hcy	Hcy
0.263270024	0.876656007	1.236010797	Hcy	Hcy
0.369384887	1.022670169	1.561100168	Cys	Cys
0.780789629	1.715166743	1.347194864	Met	Met
0.489279724	1.1851873	1.413876122	Na_2S	Na_2S
0.771633199	1.71836455	1.350988546	Met	Met
0.701600109	1.531806761	1.21412417	GSH	GSH
0.411268755	0.511192325	0.552637339	GSSG	GSSG
0.267576266	0.857297853	1.22608886	Hcy	Hcy

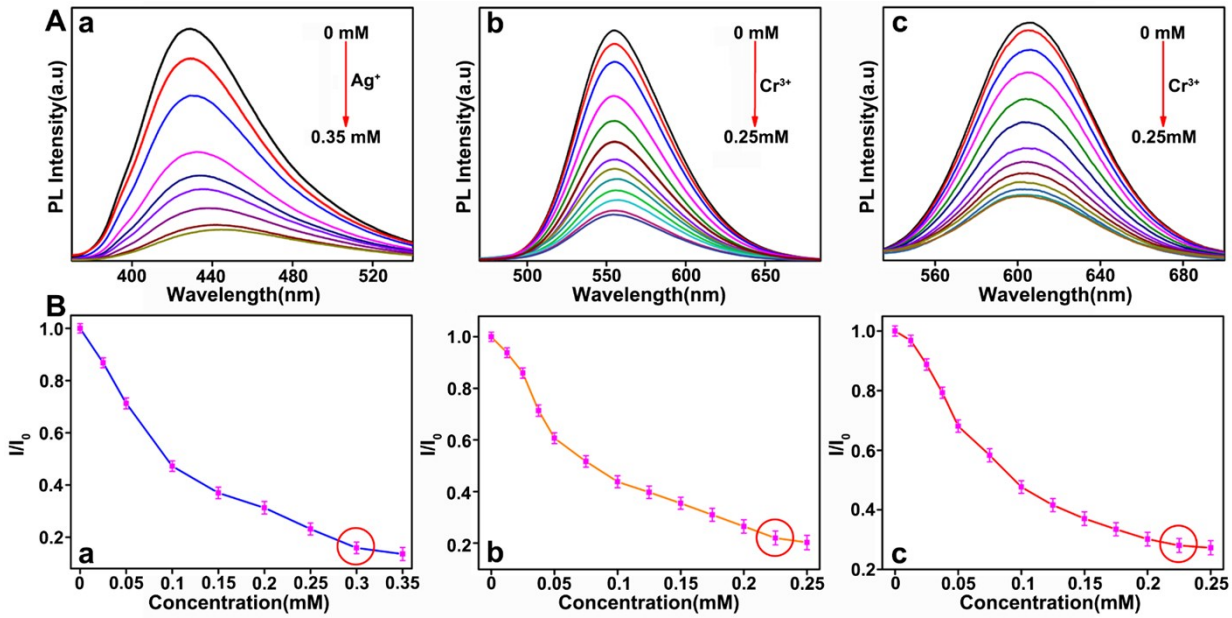

Fig. S15 Fluorescence spectra of (A-a) m-CDs in the presence of different concentrations of Ag^{+} and (A-b) o-CDs, (A-c) p-CDs in the presence of different concentrations of $Cr3^{+}$. (B-a) The relationship between I/I_0 and the concentration of Ag^{+}, where I_0 and I are the corresponding fluorescence intensities of the m-CDs in the absence and the presence of Ag^{+}, respectively. The relationship between I/I_0 and the concentration of $Cr3^{+}$, where I_0 and I are the corresponding fluorescence intensities of the (B-b) o-CDs, (B-c) p-CDs in the absence and the presence of Cr^{3+}, respectively.

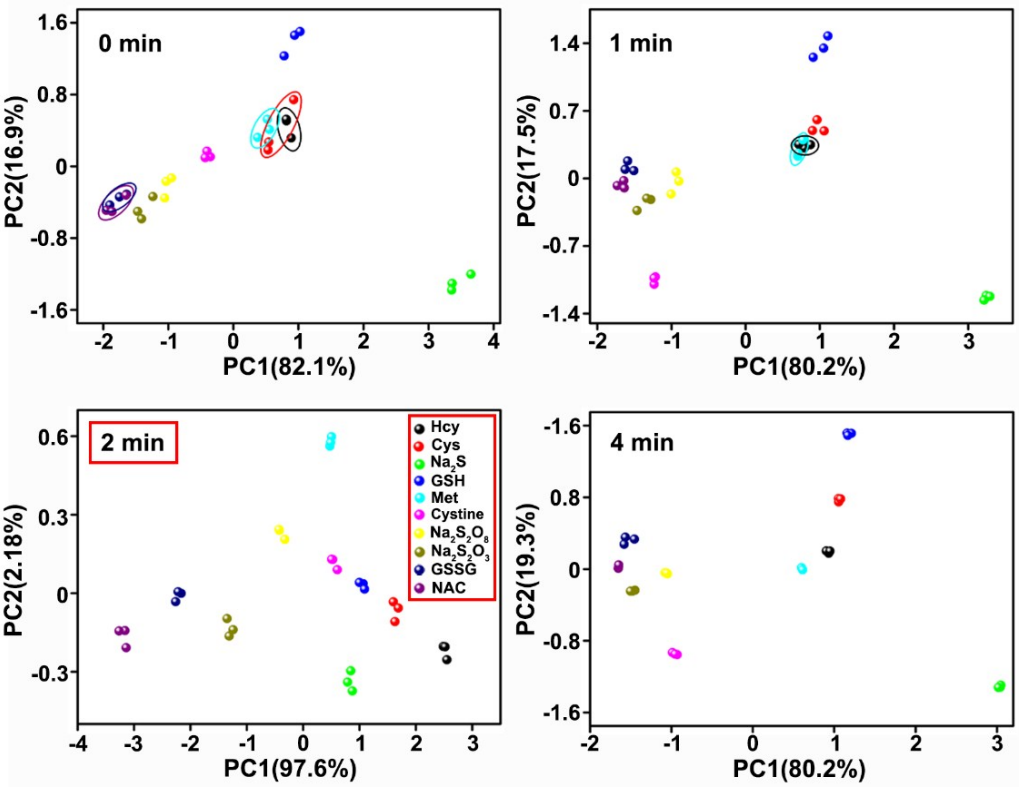

Fig. S16 The influence of response time on the sulphur-containing species discrimination.

Table S2. The assay compared with other methods for the detection of sulfur-containing species.

Methods	Response time	Reference
AuNPs/FA-AuAg NCs composite	30 min	S1
Carbon dot-metal ion pairs	30 min	S2
Urease-metal ion pairs	15 min	S3
DNA- metal ion pairs	10 min	S4
Nanozyme	20 min	S5
This work	2 min	-

S1 J. Y. Yang, T. Yang, X. Y. Wang, Y. T. Wang, M. X. Liu, M. L. Chen, Y. L. Yu, J. H. Wang, *Anal. Chem.* 2019, **91**, 6012-6018.

S2 S. Chen, C. H. Xu, Y. L. Yu, J. H. Wang, Sens. *Actuators B Chem.*, 2018, **266**, 553-560.

S3 C. Y. Lei, H. Dai, Y. C. Fu, Y. B. Ying, Y. B. Li, *Anal. Chem.* 2016, **88**, 8542-8547.

S4 H. Qiu, F. Pu, X. Ran, Y. Q. Song, C. Q. Liu, J. S. Ren, X. G. Qu, Sens. *Actuators B Chem.*, 2018, **260**, 183-188.

S5 X. Y. Wang, L. Qin, M. Zhou, Z. P. Lou, H. Wei, *Anal. Chem.* 2018, **19**, 11696-11702.

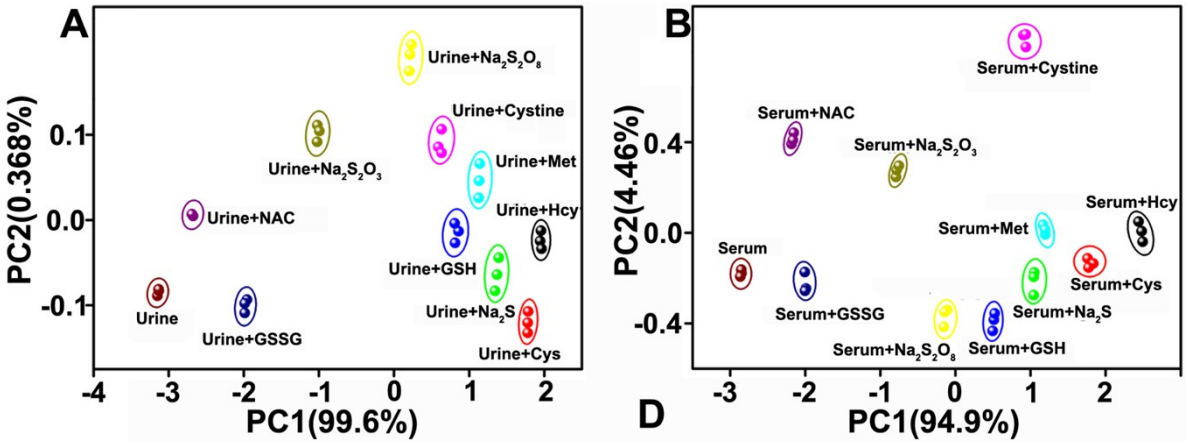

Fig. S17 PCA plot for discrimination of single sulfur-containing species in (A) human urine and (B) serum, respectively.

It's worth noting that single PCA score PC 1 or PC2 classify the different fluorescence responses produced by serums from healthy people, rectal cancer, breast cancer and prostate cancer patients with 97.8 % accuracy, demonstrating the better discrimination trends of the array based multidimensional platform (**Fig. 4A, B, D, E, G, H**). Combining both PC 1 and PC 2, the discrimination accuracy can be increased to 100%. In addition, the discrimination accuracy and sensitivity were further evaluated through receiver operator characteristic (ROC) curve analysis. The closer the line is to the upper left, the higher the sensitivity and specificity is. Generally speaking, the value of the area under ROC curve is between 0.5 (no better than chance) and 1(perfect) and greater than 0.8 is required for clinical diagnosis.[16] As shown in **Fig. 4C, F, I**, the area under ROC curve obtained according to either PC1, PC2 or PC1&PC2 are both bigger than 0.8, indicating the potential ability of the array based multidimensional platform for clinical auxiliary diagnosis.